

PULSED LASER ANNEALING OF
ION IMPLANTED GALLIUM ARSENIDE

by

ARKADY MICHAEL HORAK

B.S., Kansas State University, 1984

A MASTER'S THESIS

submitted in partial fulfillment of the
requirements for the degree

MASTER OF SCIENCE

Department of Electrical and Computer Engineering

KANSAS STATE UNIVERSITY
Manhattan, Kansas

1987

Approved by:

Andrzej Rys

Major Professor

- I. Introduction
- II. Discussion
- A. Properties of gallium arsenide
 - B. Ion implantation
 - C. Pulsed laser annealing
- III. Experiment
- A. Annealing techniques
 - B. Time resolved reflectivity
- IV. Detection of activation levels and analysis of energy threshold
- V. Conclusion
- VI. Appendix 1 Hall Effect data
- VII. Appendix 2 Time resolved reflectivity data
- VIII. References

LIST OF FIGURES

	<u>Page</u>
2.1 Zincblende lattice	7
2.2 Electronic band structure of gallium arsenide and silicon	9
3.1 Furnace diffused and ion implanted profiles	13
3.2 Implant damage caused by light and heavy ions	15
3.3 Penetration depth, R_p of implanted ions	15
3.4 Effects on implant distribution caused by channeling	17
4.1 Power density versus anneal time	19
4.2 Basic pulsed laser annealing set up	20
5.1 Raster scan annealing methods	25
5.2 Excimer laser pulse energy degradation	27
5.3 Determination of average pulse energy	27
5.4 Set up used to perform time resolved reflectivity experiments	29
6.1 Hall measurement set up	32
6.2 Sample geometries used with the Hall measurement	35
6.3 Sample used with Van Der Pauw measurement	36

I. Introduction

The processing of semiconductor materials has evolved significantly over the past several years in an attempt to satisfy current day design requirements. While the semiconductor industry still relies heavily on silicon as the chief semiconductor material, several alternate materials are now available for production use. Of primary interest is gallium arsenide (GaAs). The advantages offered by GaAs are a result of its unique properties, both electrical and optical. GaAs may become the second generation semiconductor material and eventually replace silicon in many applications.

While some of the processing techniques developed by the silicon revolution can be directly transported to GaAs production, other methods have been created solely for the processing of GaAs. Some of these techniques were available to silicon process engineers some years ago but were considered uneconomical or lacked process control. Although a gap has always existed between design and the processing of integrated circuits, the pursuit of GaAs fabrication has helped to reduce this gap by the introduction of new and more advanced processing techniques. Processes such as reactive ion etching (RIE), ion implantation, rapid thermal annealing (RTA), and chemical vapor deposition (CVD) are no longer elaborate

research methods but are requirements in achieving sub-micron device dimensions. While their introductions are primarily due to the advancement of silicon technology, some processes are a direct result of research on alternate semiconductor materials. It seems that research on GaAs processing will contribute to the development of new techniques for silicon fabrication facilities. With the advent of ion implantation as a feasible doping technique, the degree of equipment complexity has reached a new level of economic justification. One implanter may cost as much as one million dollars and yet the industry is willing to support such complex and expensive equipment in order to achieve the highest levels of circuit complexity. Pulsed laser annealing systems will almost certainly be very expensive and so the question of economic feasibility must be addressed. If such an annealing process can be developed, it must be able to compete with present day implantation and RTA methods now becoming established in fabrication lines. Therefore, there is a need to investigate the possibilities of pulsed laser annealing (PLA) and carefully weigh the advantages and disadvantages involved. The following discussion presents some of the problems associated with a PLA system and examines the methods used to determine its effectiveness. Although a study of the economics of PLA is not part of the intended scope of the research, several thoughts are included to

give the reader some idea of the support required for the PLA system.

As a substitute for furnace diffusion and implantation, and a direct replacement of rapid thermal annealing, PLA has not developed sufficiently to enter the semiconductor processing equipment market on its own. In the laboratory, small scale PLA has been successful in removing implant damage, yet a major problem remains in the application of PLA to a wider range of applications. PLA is plagued by the problem of non-uniform spatial homogeneity which is a direct result of laser beam quality. Although many applications using lasers have successfully penetrated the market, few of them require the high degree of spatial uniformity needed by PLA systems. Applications such as laser based optical communications systems circumvent this problem by using pulse coded modulation (PCM) whereby the laser source is used as a time dependent switch and very little concern is given to beam uniformity. Other examples exist that do not impose the stringent requirements of beam uniformity as does PLA. Therefore, the development of PLA systems will push laser technology to adopt new methods such as internal phase conjugation and output beam conditioning thus providing a uniform spatial intensity distribution. There are a number of other considerations to be made in the development of PLA systems

and some of these will be presented as a result of the research conducted. A brief summary of GaAs properties will precede as it is helpful in the understanding of the annealing mechanisms. Of course some measure of effectiveness is needed to establish the success of a PLA experiment so a section on the analysis and detection of activation levels is included. Experimental systems and techniques developed during the research are included for the information of those individuals willing and able to continue the investigation of pulsed laser annealing of ion implanted GaAs.

II. Discussion

A. Properties of Gallium Arsenide

Gallium (Ga) and Arsenic (As) form a III-V compound that uses a double bonding mechanism combining both ionic and covalent binding forces. A zinc blend crystal is formed as shown in figure 2.1, consisting of two interpenetrating face-centered cubic structures, one made up of Ga atoms and the other As atoms.

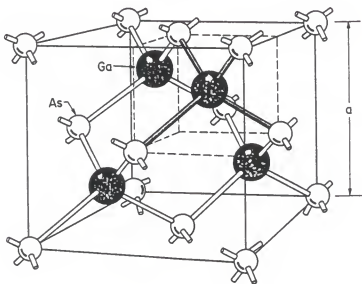


Figure 2.1

A Zincblende lattice consisting of two interpenetrating face-centered cubic structures.

Source: S.M. Sze, Semiconductor Devices, Physics and Technology, (New York: John Wiley & Sons, 1985) p. 5.

The crystal is comparable to the diamond structure of Si, but some unique properties are produced by the dissimilar atoms. GaAs ingots are produced by the Liquid Encapsulated Czochralski (LEC) method in which a seed is used to promote the growth of a crystal from a slowly rotating crucible of molten GaAs. A layer of Boric oxide is used as an encapsulant to inhibit the loss of As which tends to vaporize from the surface of the molten GaAs. The Bridgeman technique is also used to produce GaAs ingots but this method has not yielded the large diameter crystals required for full scale production of integrated circuits. Epitaxial methods are used to provide the highest quality GaAs but provide only a thin layer of material on a crystal surface. Epitaxial layers have the fewest defects and possess the best spatial qualities. Both liquid and vapor phase epitaxial techniques have been used successfully in the growth of GaAs.

The band structure of GaAs determines its major electrical and optical qualities and is shown in figure 2.2 along with the the band structure of Si. The important features of any band diagram are the location of minima in the conduction band, the slope of the band edge as it approaches the minima, and of course the band gap. The bandgap of GaAs (1.42 eV) is wider than that of Si (1.08 eV) and this gives superior high temperature device characteristics. Another result of a wider bandgap is a

lower steady state thermal recombination rate. This provides better insulating qualities and therefore good device isolation. This effect may be further enhanced to produce a semi-insulating material by the introduction of Chromium (Cr) ions in a GaAs wafer. The Cr ions form defects or trapping centers that effectively limit the steady-state recombination rate.

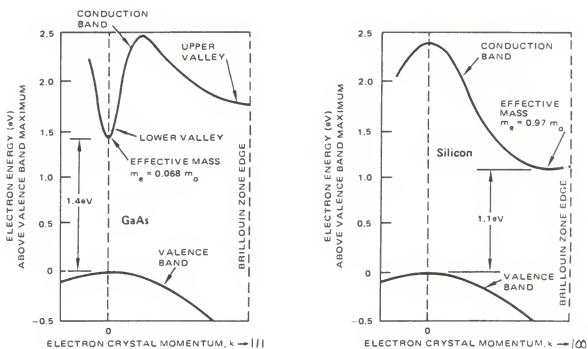


Figure 2.2

Electronic band structure of gallium arsenide and silicon in which the energy in eV is plotted against the crystal momentum k for electrons.

Source: M.J. Howes and D.V. Morgan, ed., Gallium Arsenide (New York: John Wiley & Sons, 1985) p. 521.

Devices formed on semi-insulating substrates tend to have lower leakage currents and reduced parasitic effects. The band structure diagram shows that in Si and GaAs, the highest point of the valance band is at the zero wave vector point. While the minimum of the conduction bands are not the same. GaAs is a direct bandgap material in that the conduction band minimum is at the zero wave vector point. This is not the case for Si as a change in momentum is required before recombination may occur as indicated by the shift in the conduction band minimum. The shape of the conduction band near the minimum determines the motion of electrons in the diffusion process and under applied electric fields. Under the plane wave approximation for free electrons, the mass of a particle can be determined by equation 2.1.

$$\frac{\partial^2 E}{\partial k^2} = \frac{\hbar^2}{m^*} \quad (2.1)$$

Where:

- E = energy
- k = the wave vector
- \hbar = reduced Planck constant
 $1.05458 \times 10^{-34} \text{ J-s} = \frac{h}{2\pi}$
- m^* = effective mass

The effective mass takes into account the location of a particle with respect to its location within the lattice

and therefore the effects of bonding forces and internuclear forces. The shape of the conduction band is approximated by a parabola at the minimum in this formulation. The narrower the parabola, the lower the effective mass is. Relative to Si, the effective mass of GaAs is lower. This makes electrons seem exceedingly light in GaAs and under applied electric fields, electrons are accelerated much faster than those in Si. The location of the conduction band edge in GaAs also implies good intrinsic optical absorption and luminescence processes across the band gap. Since no momentum change is required in the recombination process, lattice energy may be given off more freely in the form of photons. Optical devices should therefore be very efficient in GaAs as compared to Si.

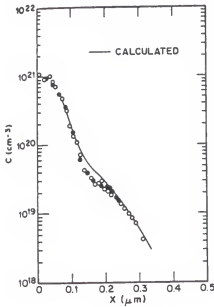
B. Ion Implantation

The introduction of impurities to produce n^+ and p^+ regions in semiconductors is accomplished by furnace diffusion or ion implantation. The former method simply drives impurities into the wafer by thermal diffusion. A layer of dopant is spun on or placed over the wafer in disc form and then put into an oven for a predetermined time. Furnace diffusion has been widely used with good success for many years but suffers from a few inherent drawbacks. During a diffusion the entire wafer must be placed into the furnace and the wafer is then totally subjected to thermal stress. There is no selectivity and diffusions from previous steps are driven in further. This can make the accurate placement of pn junctions difficult and offers limited control over the junction profile.

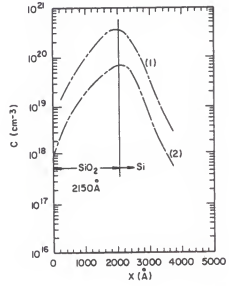
Furnace diffused profiles are zero mean processes. That is, the level at which the impurity concentration is the highest is at the surface. A wide range of profiles are obtainable by using ion implantation since impurities are selectively injected into the wafer and so the placement of the peak concentration is variable. Figure 3.1 shows a furnace diffused profile in silicon and a ion implanted profile in silicon and silicon dioxide obtained by secondary ion mass spectroscopy (SIMS) which demonstrates the ability of ion implantation to vary the

placement of the peak concentration.

Another problem associated with furnace diffusion is the out diffusion of impurities away from the intended area.



a



b

Figure 3.1

Furnace diffused (a) and ion implanted (b) profiles obtained by SIMS. Note the shift in the peak concentration in the implanted profile.

Source: S.M. Sze, ed., VLSI Technology. (New York: McGraw-Hill, 1983) p. 191.

With ion implantation, only a few straggling ions will leave the target area, which is a real improvement over conventional furnace diffusion. During subsequent

implants, other portions of the wafer remain relatively unaffected except in extreme cases where the implant dosage is so high as to cause localized heating of the wafer. The temperature of the wafer can however be carefully monitored and cooled with a cryogenic chuck if this effect influences other processes. In some circumstances, it may become desirable to hold the wafer at a high temperature and so thermal chucks have also been developed to purposely heat the wafer. Implantation is used widely in the doping of silicon wafers and is the only doping method used with GaAs since furnace diffusion has not been developed for it.

The next step in forming a doped region is to anneal the implant area. Since ion implantation is a destructive process, the crystal lattice is broken up as the high energy ions penetrate the material. When an ion enters the surface of the wafer it may collide with nuclei and thus lose some of its energy and in doing so may knock atoms out of their lattice sites. Smaller ions will not experience nuclear collisions but rather electronic interactions as they pass by the electron clouds surrounding atoms. The damage done by an ion depends on the size and velocity it has prior to impact. While a small high energy ion may penetrate quite far into the wafer, very little damage may be sustained by the crystal structure. On the other hand, larger high energy ions may collide with several nuclei near the surface and cause a great deal of crystal damage.

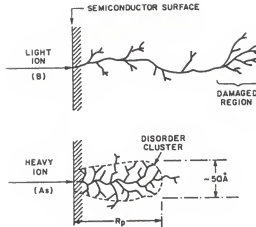


Figure 3.2

Implant disorder due to light and heavy ions.

Source: S.M. Sze, Semiconductor Devices: Physics and Technology. (New York: John Wiley & Sons, 1985.) p. 416.

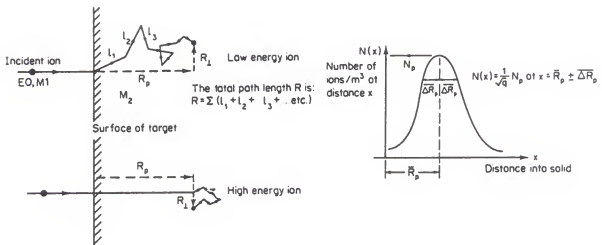


Figure 3.3

Ion range and implant distribution.

Source: M.J. Howes and D.V. Morgan, ed., Gallium Arsenide (New York: John Wiley & Sons, 1985) p. 162.

Thus the amount and location of damage is related to the size and velocity an ion possesses. Figure 3.2 shows the location of damaged regions for a light and heavy ion.

As seen in figure 3.3, the path of the ion into a wafer is not very regular and a mean implant range R_p , is shown perpendicular to the surface neglecting distances traveled transversely to the ion beam, R_t .

Extensive tables are available for determining the penetration depth of a number of different ions at different implant energies [3.1]. The orientation of the crystal with respect to the ion source also determines how far ions will penetrate and orientation along a major crystal direction will enhance the phenomena known as "channeling." This occurs when ions travel between crystal planes and are subjected to few collision or electron interactions. The result is a profile that has a tail extending into the wafer. Figure 3.4 shows what should be a normal profile but a tail is created due to channeling. Channeling may be reduced by implanting ions 7 off the major crystal axis but inevitably, some ions will experience channeling. Pre-amorphization has been used to nearly eliminate channeling by first damaging the wafer before doping thus producing a more random surface.

Once a wafer has been implanted, the crystal becomes damaged. In this phase, the material is incapable of supplying carriers to contribute to the conduction process

which was the intention of the doping. Ideally, each implanted ion should occupy a substitutional lattice site within the crystal and in doing so contribute a carrier for conduction.

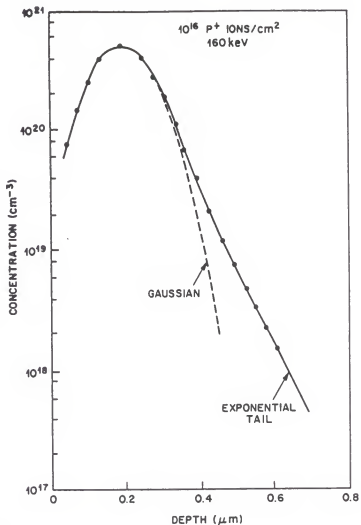


Figure 3.4

Effects on implant distribution caused by channeling.

Source: S.M. Sze, Semiconductor Devices: Physics and Technology, (New York: John Wiley and Sons, 1985) p. 413.

N-type dopants in GaAs would be elements from column VI such as Selenium (Se), Tellurium (Te), and Sulfur (S), and those from column IV, which are Silicon (Si) and Tin (Sn). P-type impurities are group III ions such as Zinc (Zn), Beryllium (Be) and Cadmium (Cd). Interestingly, silicon may act as either a p or n type dopant depending upon which of the lattice sites it occupies. If Si ions replace Ga atoms, an n-type material may be formed while a p-type material can be produced if Si ions occupy As sites.

C. Pulsed Laser Annealing

In order to complete the doping process, annealing is used to remove lattice damage caused by ion implantation. The amount of damage done by an ion is a function of the ion's size and velocity as well as the samples crystal structure and position during implantation. The degree to which an annealing process removes this damage is the best measure of its success. While furnace annealing works fairly well in activating impurities, it is not the most desirable technique to use. The wafer is subjected to long periods of thermal stress and there is no selectivity of the annealing spots as the entire wafer must be processed all at once.

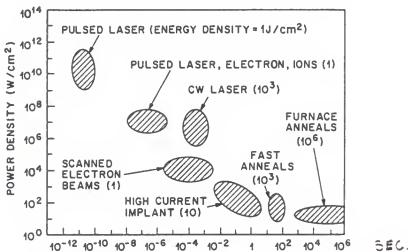


Figure 4.1

Power density versus anneal time for various annealing techniques.

Source: S.M. Sze, Semiconductor Devices: Physics and Technology. (New York: John Wiley & Sons, 1985) p. 419

Rapid thermal annealing solves the time problem by annealing wafers in a short time frame but, the method still requires the entire wafer to be heated at once.

Only pulsed laser annealing (PLA) has the ability to be the highly controllable and yet flexible annealing technique capable of satisfying the processing requirements of future device technology. Figure 4.1 shows the power density of an annealing process versus the anneal time and indicates the rapid energy transfer of pulsed laser annealing. Since the laser's energy may be directed and focused without much difficulty, a wide range of complex diffusion patterns and dimensions can be produced. Figure 4.2 is a simple annealing setup using an excimer laser to raster scan a GaAs sample. This is essentially the set-up used in this work.

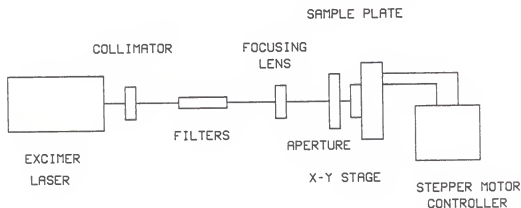


Figure 4.2

Basic set up for a raster scan anneal using an excimer laser.

Laser annealing with short pulses, known as transient annealing, has proved very successful in activating high dose implants and seems like a promising method. The exact nature of transient annealing remains controversial since it is not known if annealed material actually melts or goes through some sort of lattice softening phenomenon. A melting model [4.1] has shown good agreement with experimentally obtained data and many now agree that for GaAs, a melting phase is experienced during annealing. PLA has been used to obtain surface carrier concentrations as high as $4 \times 10^{19} \text{ cm}^{-3}$ [4.2]. In many cases, subsequent thermal processing seems to reduce the activation levels of some high dose samples. Low dose implants are not very well annealed at all and even successful high dose anneals suffer from low mobilities and the presence of high concentrations of deep levels [4.3]. The stoichiometry of surface layers has been a concern in the annealing of GaAs and the use of an encapsulant (cap) has worked well in containing arsenic that would otherwise be evolved during both rapid thermal annealing and pulsed laser annealing. However, problems occur during high energy pulses as the cap tends to blow off the sample and in addition, stress created by the cap can cause surface defects. Silicon nitride (Si_3N_4) is commonly used as an encapsulant but other materials like aluminum nitride (AlN) are thought to provide better results since its thermal expansion

coefficient is close to that of GaAs. A disadvantage of using AlN is that it is very difficult to remove from the sample since there is not a selective etch for removing it.

III. Experiment

The primary goal of this research was to investigate the effectiveness of the excimer laser as an annealing method and then develop a suitable annealing system with the equipment at hand. Many problems were encountered as research continued on pulsed laser annealing yet progress was made and data gathered that would continue to change the way the process was developed. Literature indicated that excimer laser annealing provided reasonably good activation levels [5.1] and furthermore that use of xenon chloride (XeCl) at a wavelength of 308nm seemed to be a promising starting point for an experiment. A Questek digitally controlled excimer laser and a lab facility was made available by the Center for Molecular and Solid State Energetics (MASSE) at Kansas State University. In a joint effort with members of the Physics department, PLA experiments and analysis methods were undertaken to develop a pulsed annealing method that could activate ion implanted samples of GaAs.

Early work reported by H. Yao [5.2] showed that the excimer laser could provide high levels of activation in GaAs using both single and multiple laser shots. Ideally, a pulsed annealing process should provide maximum carrier activation at the lowest possible energy in order to minimize surface damage of the sample. Yao reported that

in some cases, multiple low energy pulses were nearly equivalent to a single high energy pulse but usually the effect of a second shot, reduced the activation produced by the first. It appeared that the annealing mechanism differed slightly in the two methods and some uncertainty existed in how recrystallization occurred in the multiple shot experiments. Since the penetration depth of the excimer laser ($<150 \text{ \AA}$) was less than the projected range of the implanted impurities in GaAs, it was felt that only a shallow layer of material would become fully activated. Also, the thermal gradient in the sample was very high using the excimer laser resulting in a energy pile-up at the surface of the sample.

High energy pulses tended to remove encapsulant and early efforts were directed at establishing an energy threshold at which cap damage began to occur. It was hoped that good activation would be obtainable below this threshold so that the cap could be preserved but later the preservation of the cap was forfeited in achieving higher levels of activation. A raster scan method was adopted in which samples were annealed in an overlapping fashion. The motivation for trying this was that only a small portion of the laser beam was suitable for annealing and so it had to be scanned over large samples. The problem of non-uniform energy distribution in the laser pulse proved to be a limiting factor when the annealing of large areas was

required. In raster scanning a small spot across the sample, it was hoped that good overall uniformity would be obtained. Figure 5.1 shows two methods used to generate the raster pattern and two apertures used to mask the laser light.

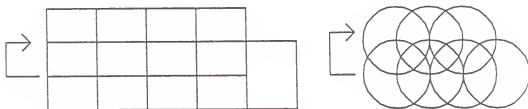


Figure 5.1

Two methods used to raster scan samples and two apertures used to select uniform portions of the laser light.

The shapes were chosen on the basis of easy area calculation and no significant difference was noticed between the two shapes. The GaAs samples were mounted on a computer controlled X-Y stage to provide the raster movement. An HP 86 was used to control a Maxwell stepper motor controller driving two Bodine stepper motors. The stages performed very well throughout the experiment and the ease of programming provided by the motor controller made the raster pattern a simple one-line command sequence. Before each sample was annealed, the laser pulses were

carefully adjusted to deliver a known energy density. This parameter was then used to establish some lower limit on the required pulse energy to notice some degree of carrier activation. It seemed that samples implanted with fluences below $1 \times 10^{14} \text{ cm}^{-2}$ did not activate very well whereas those implanted with dosages greater than $1 \times 10^{18} \text{ cm}^{-2}$ activated very well. This seemed promising for the annealing of contact areas where implant levels would be high.

Ensuring that the pulse to pulse energy of the laser was constant was important during the raster scanning but a more difficult problem was encountered in retaining pulse energies from day to day. Although the excimer laser incorporated the latest technology, such as microprocessor control and digital readout, it became a very troublesome part of the overall research. Downtime was common and the laser required constant attention to maintain its operation. Pulse energy varied daily and pulse energy fall-offs were inherent to the laser. A new gas fill provided good pulse energy for a few days but problems soon became apparent when the system began to lose more than fifty percent of its power within a week. Figure 5.2 gives some indication of the power loss problem. Pulse energy could be adjusted via the laser control panel but the addition of filters exterior to the laser were more easily adjusted and reproducible. A range of filters were chosen for each annealing experiment so that power levels could be varied

from 150 mj to about 15 mj per pulse. The power levels were monitored using a calorimeter as shown in figure 5.3.

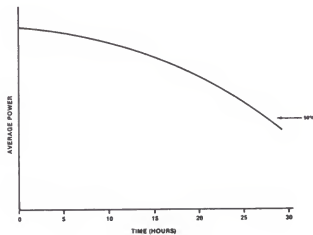


Figure 5.2

Excimer laser pulse energy fall off.

Source: Questek Excimer laser manual, 1986

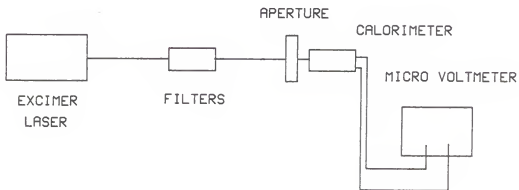


Figure 5.3

A calorimeter is used to determine the average power transmitted through an aperture of known area.

The next considerations made were those concerning the methods of testing samples to determine activation levels by means other than the previously used Raman technique. An independent method was sought that could verify the Raman results and also provide electrical characteristics such as sheet conductivity and mobility. The Hall Effect experiment was suggested for the determination of Hall mobility. A knowledge of the mobility would then give a good indication of the degree to which the sample had been annealed and thus the overall effectiveness of the annealing process.

At this point efforts were directed to the development of a suitable sample shape and the construction of a Hall Effect measurement station. A clover leaf shaped sample was then chosen to perform Van Der Pauw measurements. As mentioned earlier, the samples had to be capped in order to inhibit the loss of As as the sample was heated. The capping of the samples provided yet another problem in that the cap/sample interface was being thermally stressed and surface damage became apparent. All of the samples used in this experiment were capped with Si_3N_4 which was pyrolytically deposited to a thickness of about 60 to 80 nm. This also provided a protective coating and could eventually have been used as a mask in subsequent processing steps. Some authors suggested using a capping material that would have a closer match to the thermal

expansion coefficient of GaAs so that the stress at the sample surface would be reduced. AlN was used by some researchers [5.3] but more information is needed about its behavior before it becomes widely used. It seems that the cap becomes liquid during the annealing process and it can slide around on top of the GaAs surface without stressing it yet it still contained the As. The cap also provided a rough indication of annealing energy. In some cases the cap was completely removed.

B. Time Resolved Reflectivity

The reflectivity of a sample may be monitored during an annealing experiment using the time resolved reflectivity setup shown in figure 5.4.

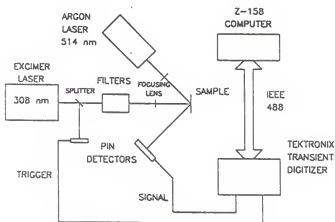


Figure 5.4

Basic setup used to perform time-resolved-reflectivity experiments.

When a laser pulse of sufficient energy strikes the surface of the sample, the change from solid to liquid or near liquid may be observed by a reflectivity probe. An argon laser (514 nm) is directed onto the sample at the same point that the excimer laser anneals a spot. The reflected argon beam is focused onto a PIN detector which monitors the intensity of the reflected light. A second PIN detector is used to trigger a transient digitizer that records the PIN signal generated by the argon laser. The digitizer is remotely programmed via the IEEE/488 bus which is controlled by a Z-158 computer. The reflectivity signal is then stored as a data file on the computer and may be recalled for plotting at a later time. Experiments were conducted on capped and bare GaAs to determine the effects of Si_3N_4 caps on pulsed laser annealing. Reflectivity signals obtained during the experiment are contained in Appendix 2. Reflectivity information can be used to determine the melt duration and length of melt phase of a sample during a pulsed anneal. The change in signal amplitude indicates the relative change in reflectivity while its duration, once the annealing source is removed, indicates the time for the material to refreeze. These features are dependent upon many factors such as pulse duration, wavelength and waveshape as well as the melting temperature and thermal conductivity of the sample.

In some instances, the cap may vaporize during an

anneal resulting in a reflectivity plot that does not return to its initial level. The melting point of Si_3N_4 is about 150 to 200 degrees Celcius higher than that of GaAs so a liquid phase may exist beneath the cap at temperatures between 1700 and 1900 degrees Celsius. This may be observed in a reflectivity plot as one can discern a solid phase and liquid phase reflectivity level.

In experiments conducted here, the excimer laser could penetrate about 150 Å while the argon laser could probe 55nm into the sample. The thickness of the cap must be taken into account and may be determined by ellipsometry. Samples obtained from Honeywell contained about 75 to 80 nm of Si_3N_4 while those from Wright Patterson AFB were only 60 nm thick. The reflectivity probe gives real-time or time-resolved information about the reflectivity of an annealed sample and thus serves as a valuable tool in the analysis of the annealing mechanism.

VI. Analysis and detection of activation levels

The Hall Effect is used to determine carrier type and concentration. Figure 6.1 shows the basic test setup used to determine the Hall voltage (V_H) from which the Hall mobility (μ_H) is calculated. A constant current is established along one axis of the sample while a magnetic field is applied perpendicularly to the current flow. This establishes the Lorentz force as given by equation 6.1.

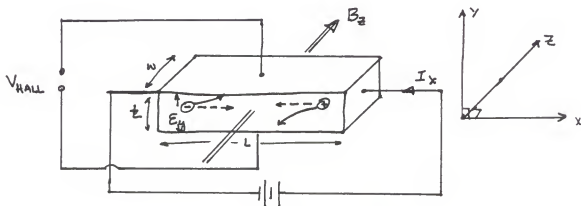


Figure 6.1

Basic Hall measurement set-up.

Holes moving through the sample are subjected to the Lorentz force which tends to force them towards the bottom of the sample as they are swept to the the lower potential. Electrons of course, are pushed upward.

$$F_y = q (E_y - V_x B_z) \quad (6.1)$$

The result of the Lorentz force is to produce a vertical electric field E_y as in equation 6.2 that acts to balance the $V_x B_z$ product so that the net force on carriers is zero.

$$E_y = V_x B_z \quad (6.2)$$

The potential developed across the semiconductor as a result of this balancing field is known as the Hall voltage. To find the relationship between Hall voltage and the carrier concentration, we begin by describing the current density as in equation 6.3.

$$J_p = q p V_p = q p \mu_p E \quad (6.3)$$

The current density J_p , is defined as the number of carriers crossing a unit area per unit time multiplied by the charge q . Substituting 6.3 into 6.2, we get equation 6.4.

$$E_y = J_x \times \frac{B_z}{q p_0} = R_H J_x B_z \quad (6.4)$$

$$\text{where } R_H = \frac{1}{q p_0}$$

R_H is called the Hall coefficient and is the proportionality constant relating the current density and magnetic flux density through the sample. Manipulating terms, equation 6.5 gives a value for the hole concentration, p_0 , for a known current, B field and Hall voltage.

$$p_0 = \frac{1}{qR_H} = \frac{J_x B_z}{qE_y} = \frac{(I_x/wt)B_z}{q(V_{AB}/w)} = \frac{I_x B_z}{qtV_{AB}} \quad (6.5)$$

By obtaining a resistance measurement, the resistivity of the sample may be determined as in equation 6.6.

$$\rho \text{ (}\Omega\text{-cm)} = \frac{Rwt}{L} = \frac{V_{cd} / I_x}{L / wt} \quad (6.6)$$

The Hall mobility is then defined as the product of the Hall coefficient and the conductivity.

$$\mu_p = \sigma / qp_0 = \sigma R_H \quad (6.7)$$

The carrier type is determined by the sign of the Hall voltage, where positive represents p-type and negative n-type for the current and B-field conventions used above. The accuracy of the Hall voltage is dependent largely upon the geometry of the sample and the size of the contacts.

The effects of contact size can be minimized by using one of the geometries shown in figure 6.2.

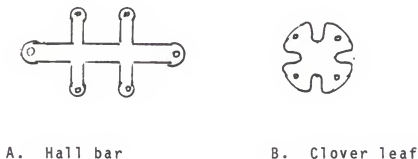


Figure 6.2

Sample geometries used with Hall measurements.

The bridge-type sample is also good for low temperature measurements but, it can be difficult to cut such a geometry out of a wafer. The clover pattern was indirectly used in an annealing experiment by producing the pattern on a semi-insulating GaAs wafer via a mask. In this fashion the pattern was not actually cut from the wafer but the semi-insulating substrate formed its boundaries.

An alternate Hall measurement technique was used to accommodate irregular sample shapes and has been successfully implemented on furnace-annealed samples [6.1]. Contact points are made at four points on the periphery on the sample as in figure 6.3. Current leads are connected to points M,O and a resistance measurements is made at points N,P and is denoted $R_{MO,NP}$.

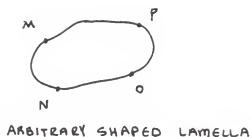


Figure 6.3

Sample geometry used with Van der Pauw measurements.

A B-field is then applied at right angles to the current flow and another resistance measurement is made. A change in resistance, $R_{MO,NP}$ is then used to calculate the Hall coefficient as in equation 6.8.

$$R_H = \frac{t}{B} R_{MO,NP} \quad (6.8)$$

This method requires that the contacts are sufficiently small compared to the sample size, they are located on the periphery of the sample, and the sample is of uniform thickness (t) and free of holes. Also, the current stream lines in the sample must not change when the magnetic field is applied. This last stipulation implies that following

the application of the B-field, the electric field changes as there is an added transverse component compensating the induced Lorentz force. This is also the case for the conventional Hall measurement.

V. Conclusion

Pulsed laser annealing can provide good activation of implanted GaAs but some problems exist in applying this technique to large annealing areas. While many types of laser have been used to perform annealing, the excimer laser seems to be more efficient in removing implant damage. The large cavities found in most excimers can support many oscillations and should therefore provide a homogenous output beam. However, we found the degree of homogeneity is still not acceptable. Spot sizes on the order of 1 to 2 mm cannot be used effectively in a production environment and some method of homogenization is required before pulsed annealing can be adopted as a viable technique. The raster scanning method of annealing produced irregularly activated regions where overlapping patterns were present and amorphous regions when the aperture did not overlap. The resulting material would contain areas of low mobility and thus poor device performance. Accurate methods of determining activation levels are available and do not pose a problem to the development of laser annealing but the procurement of such equipment may be limited by economic considerations. The most crucial aspect of pulsed laser annealing is the understanding of the annealing mechanism and a knowledge of the interaction between the laser and the sample. While

activation can be achieved and a high degree of implant damage removed, very little is known about transient annealing and therefore continued research is required to characterize this process.

Appendix A
Hall Effect Data

Hall Effect data run #1

B = 1.0 Tesla

I μ a	V _{forward}	V _{reverse}	Static _f	Static _r
1.0	0.736	-0.736	0.66	-0.66
3.0	2.2	-2.2	1.99	-1.99
10.0	7.36	-7.36	6.65	-6.65
30.0	22.1	-22.1	19.96	-19.97
100.0	73.56	-73.7	66.51	-66.63

Reverse B field

1.0	0.591	-0.592	0.662	-0.664
3.0	1.77	-1.77	1.99	-1.99
10.0	5.91	-5.91	6.64	-6.64
30.0	17.73	-17.74	19.92	-19.93
100.0	59.06	-59.16	66.33	-66.45

Hall Effect data run #2

B = 2.0 Tesla

I μ a	V _{forward}	V _{reverse}	Static _f	Static _r
1.0	0.808	-0.809	.664	-.666
3.0	2.42	-2.42	1.99	-2.00
10.0	8.09	-8.09	6.65	-6.66
30.0	24.25	-24.27	19.96	-19.97
100.0	80.77	-80.93	66.49	-66.62

Reverse B field

1.0	0.518	-0.519	0.662	-0.664
3.0	1.55	-1.55	1.99	-1.99
10.0	5.19	-5.19	6.64	-6.64
30.0	15.56	-15.56	19.90	-19.91
100.0	51.82	-51.9	66.28	-66.39

Hall Effect data run #3

B = 3.0 Tesla

I μ a	V _{forward}	V _{reverse}	Static _f	Static _r
1.0	0.446	-0.447	0.662	-0.664
3.0	1.34	-1.34	1.99	-1.99
10.0	4.47	-4.47	6.63	-6.63
30.0	13.40	-13.41	19.86	-19.96
100.0	44.63	-44.70	66.25	-66.36

Reverse B field

1.0	0.880	-0.881	0.664	-0.666
3.0	2.64	-2.64	1.99	-2.00
10.0	8.80	-8.81	6.65	-6.65
30.0	26.41	-26.42	19.95	-19.96
100.0	87.94	-88.13	66.46	-66.61

Hall Effect data run #4

B = 4.0 Tesla

I μ a	V _{forward}	V _{reverse}	Static _f	Static _r
1.0	0.951	-0.955	0.664	-0.667
3.0	2.86	-2.86	2.00	-2.00
10.0	9.54	-9.54	6.66	-6.67
30.0	28.62	-28.63	19.99	-20.00
100.0	95.28	-95.48	66.59	-66.72

Reverse B field

1.0	0.373	-0.378	0.662	-0.666
3.0	1.13	-1.13	1.99	-1.99
10.0	3.75	-3.75	6.64	-6.64
30.0	11.26	-11.26	19.92	-19.93
100.0	37.50	-37.55	66.32	-66.40

Hall Effect data run #5

B = 5.0 Tesla

I μ a	V _{forward}	V _{reverse}	Static _f	Static _r
1.0	1.03	-1.03	0.665	-0.668
3.0	3.08	-3.08	2.00	-2.00
10.0	10.27	-10.27	6.66	-6.67
30.0	30.80	-30.82	19.99	-20.00
100.0	102.56	-102.79	66.60	-66.73

Reverse B field

1.0	0.300	-0.306	0.663	-0.666
3.0	0.906	-0.910	1.99	-1.99
10.0	3.03	-3.03	6.64	-6.64
30.0	9.08	-9.08	6.64	-6.64
100.0	30.25	-30.27	66.33	-66.44

Hall Effect data run #6

B = 6.0 Tesla

I μ a	V _{forward}	V _{reverse}	Static _f	Static _r
1.0	1.10	-1.10	0.665	-0.668
3.0	3.30	-3.30	2.00	-2.00
10.0	11.01	-11.01	6.67	-6.67
30.0	33.02	-33.04	20.00	-20.00
100.0	109.94	-110.19	66.23	-66.75

Reverse B field

1.0	0.227	-0.230	0.662	-0.666
3.0	0.687	-0.690	1.99	-1.99
10.0	2.29	-2.29	6.64	-6.64
30.0	6.88	-6.88	19.91	-19.93
100.0	22.93	-22.95	66.30	-66.45

Hall Effect data run #7

B = 7.0 Tesla

$I \mu\text{a}$	V_{forward}	V_{reverse}	Static_f	Static_r
1.0	1.17	-1.18	0.664	-0.668
3.0	3.52	-3.53	2.00	-2.01
10.0	11.76	-11.76	6.67	-6.67
30.0	35.3	-35.3	20.00	-20.01
100.0	117.47	-117.74	66.63	-66.76

Reverse B field

1.0	0.154	-0.157	0.663	-0.664
3.0	0.460	-0.466	1.99	-1.99
10.0	1.54	-1.54	6.64	-6.64
30.0	4.63	-4.63	19.91	-19.92
100.0	15.44	-15.44	66.30	-66.47

Hall Effect data run #8

B = 8.0 Tesla

I μ a	V _{forward}	V _{reverse}	Static _f	Static _r
1.0	1.25	-1.28	0.664	-0.669
3.0	3.76	-3.76	2.00	-2.01
10.0	12.54	-12.54	6.699	-6.675
30.0	37.60	-37.63	20.02	-20.03
100.0	125.2	-125.5	66.7	-66.8

Reverse B field

1.0	0.076	-0.080	-0.661	-0.667
3.0	0.230	-0.236	1.99	-1.99
10.0	0.776	-0.779	6.64	-6.43
30.0	2.34	-2.34	19.92	-19.93
100.0	7.80	-7.78	66.3	-66.3

Hall Effect data run #9

B = 9.0 Tesla

I μ a	V _{forward}	V _{reverse}	Static _f	Static _r
1.0	1.33	-1.33	0.667	-0.666
3.0	3.99	-4.00	1.99	-2.00
10.0	13.33	-13.33	6.67	-6.66
30.0	39.97	-40.00	20.00	-20.01
100.0	133.1	-133.4	66.65	-66.79

Reverse B field

1.0	-0.002	-.002	0.665	-0.662
3.0	-0.002	-0.001	1.99	-1.99
10.0	-0.003	-0.003	6.64	-6.64
30.0	-0.01	0.01	19.90	-19.92
100.0	-0.02	0.053	66.26	-66.40

Hall Effect data run #10

B = 10.0 Tesla

I μ a	V _{forward}	V _{reverse}	Static _f	Static _r
1.0	1.41	-1.42	0.665	-0.668
3.0	4.24	-4.24	2.00	-2.00
10.0	14.14	-14.15	6.674	-6.76
30.0	42.43	-42.46	20.01	-20.02
100.0	141.28	-141.63	66.66	-66.82

Reverse B field

1.0	-0.083	0.077	0.664	-0.666
3.0	-0.243	0.239	1.99	-1.99
10.0	-0.810	0.806	6.43	-6.47
30.0	-2.42	2.43	19.92	-19.93
100.0	-8.06	8.10	66.33	-66.42

All

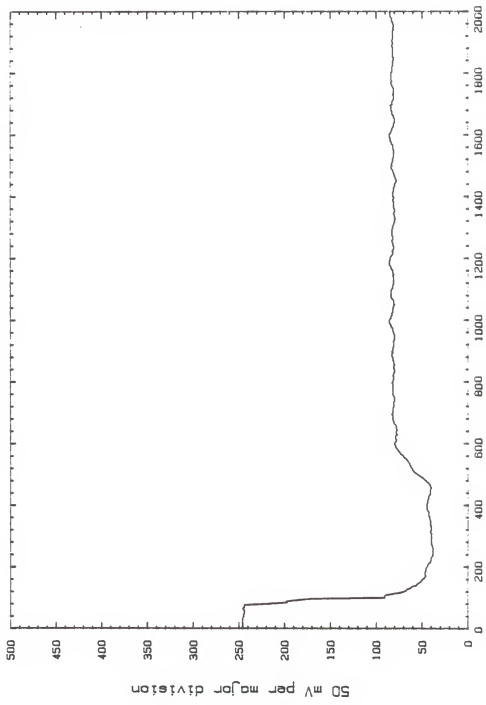
Appendix B

Time Resolved Reflectivity Data

The TRR plots show relative changes in the reflectivity of pulsed annealed samples. The vertical axis of the plot is reflectivity relative to an initial zero-time measurement. The units are arbitrary but may be scaled if required. All TRR plots are zeroed about the center of the vertical axis and changes in the signal are measured relative to this point. The x-axis is time and is labeled in all plots.

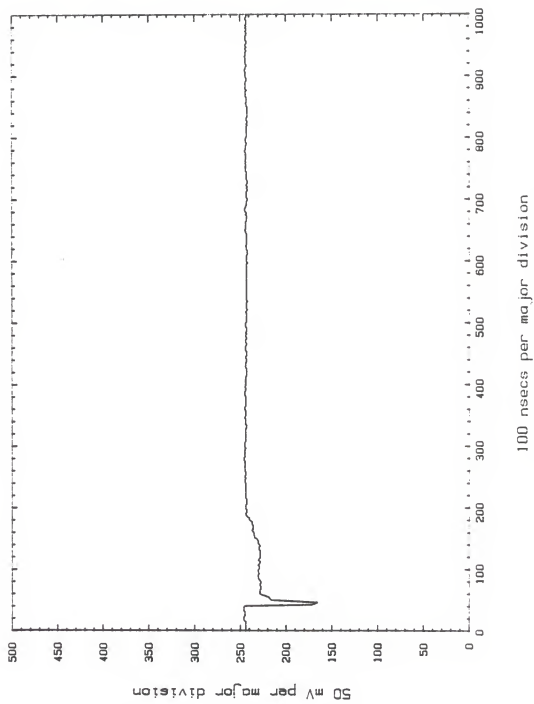
The reflectivity begins at some base level before a pulsed anneal occurs. As the excimer laser triggers a transient digitizer at the onset of annealing, the reflectivity of the sample changes. The signal may shift up or down depending on the polarity of the detector but in the plots here, the shift downward represents an increase in reflectivity. During some experiments, the encapsulant may have been removed and therefore, the reflectivity will not have returned to its initial level. A permanent shift in the TRR plot indicates a change in the surface properties of the sample. Only two distinct levels are seen in the plots and these correspond to a solid and liquid phase of the sample. The slopes and width of the pulse can give information about the melting and freezing processes taking place during annealing.

Filename: gaas2a.dat

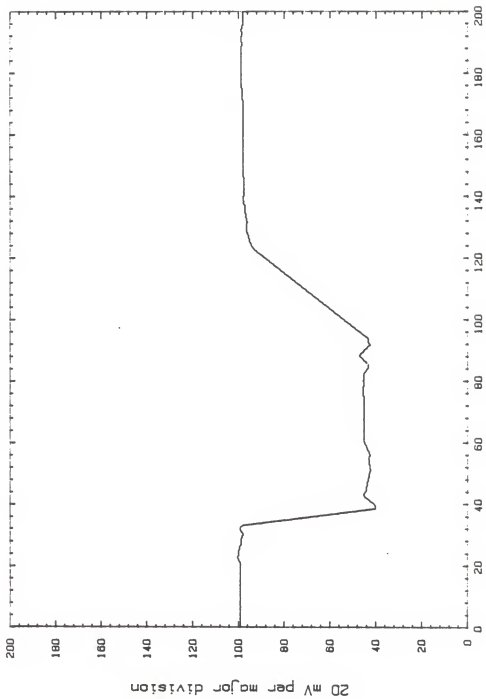


200 nsecs per major division

Filename: gaas2b.dat

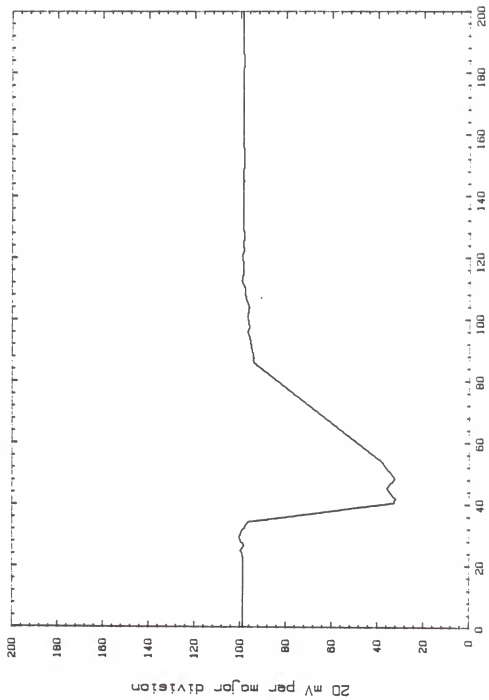


Filename: gaas2c.dat



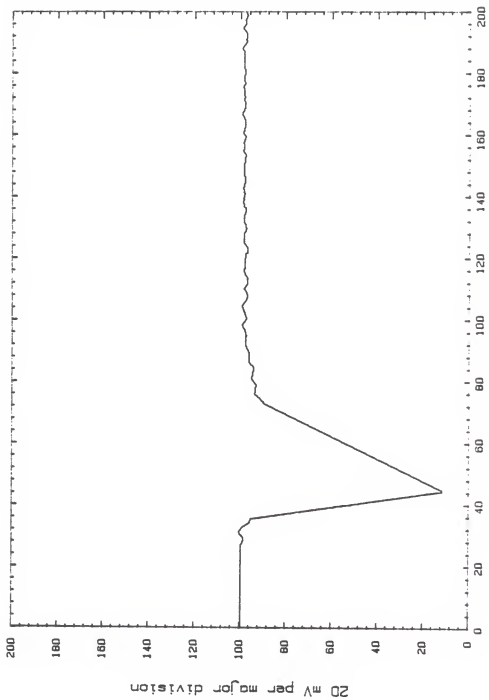
20 nsacs per major division

Filename: gaas2d.dat

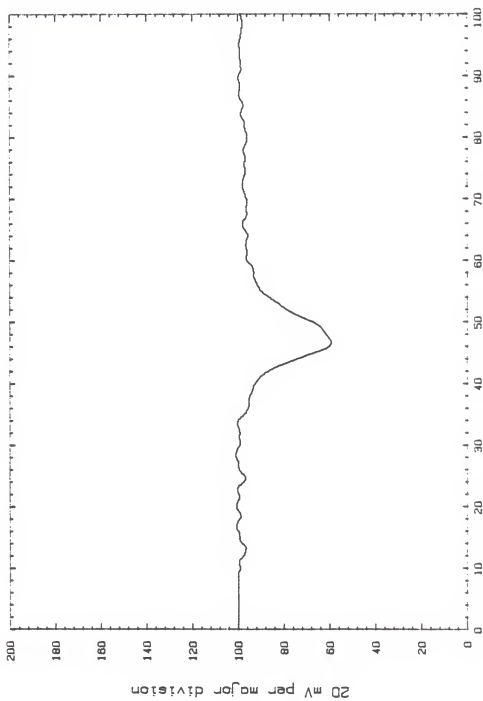


20 nsecs per major division

Filename: gaas2e.dat

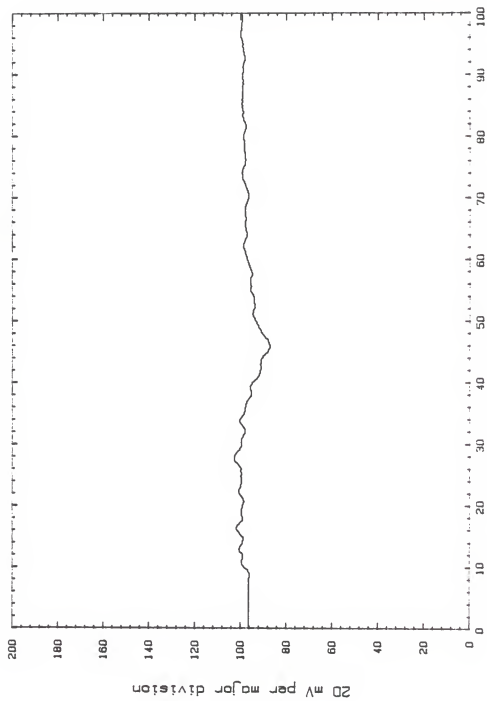


Filename: gaas2f.dat



10 nsacs per major division

Filename: gaas2g.dat



REFERENCES

- 3.1 James Gobbons et al., Projected Range Statistics Dowden, Hutchinson & Ross, Inc.
- 4.1 R.F. Wood, G.E. Giles, Phys. Rev. B 23, 1981, p. 2923.
- 4.2 C.W. White, P.S. Peercy, eds., Laser and Electron Beam Processing of Materials (New York: Academic, 1980), p. 328-33.
- 4.3 S. Nojima, J. Appl. Phys. 53(7), 1982. p. 5028.
- 5.1 R.T. Young et al., Solid State Technology, Nov. 1983.
- 5.2 H. Yao, A Masters thesis. Kansas State University. 1983.
- 5.3 H. Nishi et al., AlN Encapsulant for Fabrication of Implanted GaAs IC, Proceedings of the International Symposium on Gallium Arsenide and Related Compounds. Sept. 20-23, 1981.
- 6.1 L.J. van der Pauw, Phillips Tech. Rev. Vol. 20. 1958, pp. 220-24.

PULSED LASER ANNEALING OF
ION IMPLANTED GALLIUM ARSENIDE

by

ARKADY MICHAEL HORAK

B.S., Kansas State University, 1984

AN ABSTRACT OF A MASTER'S THESIS

submitted in partial fulfillment of the
requirements for the degree

MASTER OF SCIENCE

Department of Electrical and Computer Engineering

KANSAS STATE UNIVERSITY
Manhattan, Kansas

1987

Abstract

This thesis reports research conducted on pulsed laser annealing of gallium arsenide (GaAs) and details the experiments used for post annealing analysis. The electronic properties of GaAs are presented and a brief explanation of ion implantation is included. An excimer laser containing xenon chloride at a wavelength of 308 nm was used as an annealing source. Several annealing techniques were investigated and special fixtures were constructed to implement them. A Hall Effect measuring station was assembled for determining the activation levels in annealed samples in order to confirm the results obtained by co-workers using Raman analysis. Time resolved reflectivity experiments were conducted to determine the impact of the annealing process on the encapsulant and investigate the effects the encapsulant had on annealing. Characterization of the laser source showed poor spatial uniformity and therefore reduced the overall effectiveness of the annealing process. Pulsed laser annealing of small spots provided good activation levels in heavily doped samples but a successful procedure for the annealing of larger areas was not found.